CHAPTER- 4

Fabrication of dopamine sensor based on a carbon paste electrode modified with tetracyanoquinodimethane and cobalt tungstate nanoparticles

4.1 Introduction

Dopamine (DA) is a biologically active molecule and one of the essential neurotransmitters in animals, including humans, that plays several vital roles in learning, memory, emotion control, and cognition [1]. Therefore, abnormalities and little bit changes in the concentration of DA may cause mental and neurological disorders, including depression, dependence, Parkinson's disease, Schizophrenia, and Alzheimer's disease [2,3]. So, selective and sensitive approaches are needed to determine the dopamine level in the human body to diagnose disease and pathology research. In previous years, detection technologies have played an essential role in developing clinical diagnosis, disease treatment, and anti-cancer drugs. Techniques like electrochemical methods [4,5], surface plasmon resonance [6], high-performance liquid chromatography [7], fluorescence [8,9], photoelectrochemical sensor [10,11], colorimetry [12,13], and chemiluminescence [14] have been developed for the identification and quantification of dopamine. In the above-discussed methods, the electrochemical method is better than other methods because other methods are more expensive, take longer time, and are inconvenient to prepare. On the other hand, due to the electroactive nature of dopamine, electrochemical techniques offer an easy, sensitive, low-cost, and rapid investigation of dopamine.

The carbon materials were used with various metal nanoparticles for the fabrication of a modified carbon paste electrode [15]. Nanomaterials have been developed as possible electrode modifiers for electrochemical sensors. The nanostructure of binary metal oxides has received much interest in electrochemical sensor construction

in the past few years because of their superior electrocatalytic activity, large surface area, high conductivity, chemical stability, and inexpensive cost with respect to noble metals. The binary metal tungstate (MWO_4) exhibits outstanding physicochemical characteristics, such as natural abundance, high redox activity, excellent surface area, and improved electrochemical efficiency [16]. Based on bivalent cation, the atomic structure of a crystal of metal tungstate is categorized into wolframite and scheelite, which is discussed in previously reported articles. The larger M^{2+} cations (M = Mg, Ca, & Ba) show scheelite tetragonal structure, while smaller M^{2+} cations (M = Mn, Fe, Co & Zn) show wolframite monoclinic structure [17]. Cobalt tungstate is a wolframite monoclinic structure in which cobalt is stable in a Co^{2+} oxidation state while tungsten is in a W^{6+} oxidation state [18]. Cobalt tungstate (CWO) is widely used in various applications, such as supercapacitors [19], photocatalytic degradation [20], batteries [21,22], sensors [23], and electrochemical water splitting [24]. CWO has attracted widespread attention as an excellent sensor electrocatalyst due to its unique magnetic, optical, and thermal properties, high electrical conductivity, low toxicity, and environmental characteristics [25]. CWO is synthesized in various ways, including molten salt processes [26], sonochemical treatment [27], microwave routes [28], solvent methods [29], spray pyrolysis [30], chemical precipitation techniques [31], and hydrothermal methods [32,33]. Here we synthesize $CoWO_4$ nanoparticles by hydrothermal method which is used to fabricate dopamine sensors. The synthesized $CoWO_4$ nanoparticles were characterized by scanning electron microscopy (SEM), transmission electron microscopy (TEM), X-ray diffraction (XRD), and X-ray photoelectron spectroscopy. 7,7,8,8-Tetracyanoquinodimethane (TCNQ), is a highly versatile molecule that acts as a very

potent organic electron acceptor [34-36]. This is attributed to its planar backbone and the presence of four cyano groups, which give it a high electron affinity of around 2.8 ± 0.1 eV. It is often utilized in organic charge-transfer salts to enhance their electrical conductivity. Some TCNQ-based charge transfer (CT) salts, such as tetrathiafulvalene (TTF)-TCNQ, have an electrical conductivity that is similar to metals [37].

In this paper, we have designed TCNQ@$CoWO_4$/CPE by physical grinding of TCNQ with $CoWO_4$ in a mortar with pastel, and the TCNQ@$CoWO_4$ complex is formed. The specific goal of using the combination of TCNQ and $CoWO_4$ is to enhance the performance of the electrode. $CoWO_4$ shows less electrocatalytic activity when we combine TCNQ with $CoWO_4$ due to synergistic interaction electrocatalytic activity increases. TCNQ facilitates fast electron transfer, while $CoWO_4$ provides additional catalytic sites, both working together and improving the surface area, electrocatalytic activity, and stability of the electrode. The enhanced surface area provides more accumulation of dopamine on the electrode surface due to this reason electrochemical studies with modified TCNQ@$CoWO_4$/CPE provide good sensitivity, high peak current, low charge transfer resistance, low detection limit, better stability, and good reproducibility.

4.2 Experimental

4.2.1 Chemicals

Tetracyanoquinodimethane (TCNQ), hydrochloric acid (HCl), graphite powder (particle size < 20 µm), and Nujol oil (density 0.838 g/mL) were bought from Sigma Aldrich. Sodium tungstate dihydrate ($Na_2WO_4.2H_2O$), cobalt nitrate hexahydrate

($Co(NO_3)_2.6H_2O$), dopamine ($C_8H_{11}NO_2$), sodium hydroxide (NaOH), disodium hydrogen phosphate (Na_2HPO_4), monosodium dihydrogen phosphate (NaH_2PO_4), and melting point capillaries were bought from Sisco Research Laboratories (SRL) Pvt. Ltd.

4.2.2 Synthesis of $CoWO_4$ nanoparticles

The $CoWO_4$ nanoparticle was synthesized using a previously reported method with slight modification. In brief, 291.03 mg of cobalt chloride hexahydrate was dissolved in 30 ml deionized (DI) water in a 50 ml beaker and stirred for 15 minutes. In another beaker, 293.82 mg $Na_2WO_4.2H_2O$ was solvated in 30 ml deionized (DI) water and spun for 15 minutes on a magnetic stirrer. Now, sodium tungstate dihydrate solution was added dropwise to cobalt chloride hexahydrate solution under stirring conditions. After then mixture solution pH was adjusted to 8.0 by adding 1.0 M NaOH solution dropwise drop and stirred the solution for one hour. Then, the mixture of sodium tungstate dihydrate and cobalt chloride hexahydrate solution was transferred to a teflon autoclave and heated at 160 ℃ for 8 hours in a muffle furnace. The autoclave was cooled down at room temperature, which resulted in a light brown color $CoWO_4$ precipitate obtained at the bottom of the autoclave. The obtained precipitate was washed with DI water 4-5 times, followed by ethanol washing, then centrifuged and dried at 60 ℃ for 6 hours in a vacuum oven. The obtained $CoWO_4$ powder was calcined at 500 ℃ in the furnace for 5 hours to form the $CoWO_4$ nanoparticle.

4.2.3 Characterization instruments

The crystalline nature of the as-synthesized material was confirmed by Bench Top X-ray diffraction (BT-XRD) using a Rigaku Miniflex 600 Desktop X-ray diffraction system

HyPix-400 MF (2D HPAD) detector. The existence of cobalt, tungsten, and oxygen elements in the $CoWO_4$ was confirmed with the K-Alpha X-ray photoelectron spectrometer system (Thermo Fisher Scientific USA). The structural morphology and size of $CoWO_4$ were clearly observed by scanning electron microscopy (EVO- scanning electron microscope MA 15/18 CARL ZEISS MICROSCOPY LTD) and transmission electron microscopy (Tecnai G2 20 TWIN, FEI Company of USA (S.E.A.) PTE, LTD), respectively.

CH instrument 608C USA was used for electrochemical characterization, such as cyclic voltammetry (CV), amperometry, differential pulse voltammetry (DPV), and electrochemical impedance spectroscopy (EIS), using a 2 mL cell with a three-electrode system. The TCNQ@$CoWO_4$/CPE as the working electrode, Ag/AgCl (RE 1B ALS Co. Ltd, Japan), and the platinum electrode were used as reference and counter electrodes. All electrochemical experiments in the manuscript have been performed with Ag/AgCl reference electrodes.

4.2.4 Fabrication of TCNQ@$CoWO_4$/CPE

The TCNQ@$CoWO_4$/CPE was fabricated by mixing graphite powder, TCNQ, and $CoWO_4$ in a mortar; after that few drops of nujol oil were added, resulting in a homogeneous mixture. This homogeneous mixture was smoothed on clean butter paper, and a paste was obtained. Now, this paste was filled in melting point glass capillaries, a copper wire was connected, and the electrode was ready for electrochemical analysis. The composition of the modified electrode is shown in Table 4.1

Table 4.1 Composition of the modified carbon paste electrodes.

System	TCNQ (w/w) %	$CoWO_4$ (w/w) %	Graphite (w/w) %	Nujol oil (w/w) %
CPE	-	-	75.00	25.00
TCNQ/CPE	2.00	-	73.00	25.00
TCNQ@$CoWO_4$/CPE	2.00	10.00	63.00	25.00

4.3 Results and Discussion

4.3.1 XRD, XPS, SEM, and TEM analysis of $CoWO_4$ nanoparticles

Powder X-ray diffraction analysis was used to evaluate the crystalline characteristics, structural inspection, and phase uniformity of $CoWO_4$ nanoparticles. The X-ray diffraction distribution pattern of $CoWO_4$ nanoparticles is shown in Figure 4.1. Peaks in the diffraction pattern are situated at 2θ = 15.57°, 18.97°, 23.91°, 24.71°, 30.64°, 31.45°, 36.39°, 38.58°, 41.34°, 44.51°, 45.91°, 48.87°, 50.64°, 52.08°, 54.03°, 61.78°, 63.82°, 65.12°, 68.70°, 71.85° has been assigned to (010), (001), (-110), (011), (-111), (020), (200), (002), (-201), (-211), (-112), (-220), (022), (031), (-122), (-311), (222), (- 231), (-140) and (-123) planes of $CoWO_4$, respectively. The diffraction spectra shown in the XRD image are well-matched to the JCPDS file number 15-0867 [38]. All the peaks in the XRD spectra are sharp and narrow, indicating that the nanoparticles are highly crystalline. No additional peaks were visible, suggesting the excellent purity of the sample.

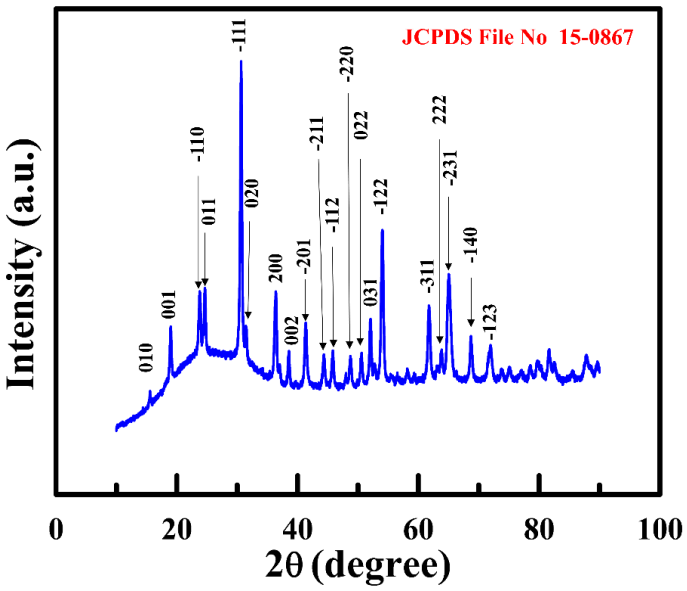

Figure 4.1 XRD spectrum of $CoWO_4$ nanoparticles.

The XPS approach was used to examine the oxidation states and chemical composition of the as-synthesized cobalt tungstate. As shown in Figure 4.2 (a), the XPS survey spectrum of cobalt tungstate includes cobalt, tungsten, and oxygen elements. The binding energies of Co 2p, W 4f, and O 1s as shown in Figure 4.2 (b-d) have been adjusted using XPS peak 41 software. Figure 4.2 (b) demonstrates the binding energies of Co 2p at 780.7 eV, 782.5 eV, 787.1 eV, and 796.8 eV are related to the Co $2p_{3/2}$ and Co $2p_{1/2}$, and the satellite peaks at 798.7 eV, and 803.6 eV represent the Co $2p_{3/2}$ and Co $2p_{1/2}$, validating the oxidation states of Co^{2+} and Co^{3+} [39], respectively. After fitting the XPS spectra, two binding energy peaks of W 4f appeared at 35.2 eV and 37.3 eV as exhibited in Figure 4.2 (c). These peaks correspond to W $4f_{7/2}$ and W $4f_{5/2}$, which shows that W 4f is present in the W^{6+} oxidation state [40]. In the cobalt tungstate nanoparticles, O 1s illustrate two independent binding energies at 530.6 eV for metal-oxygen (M-O) and

531.9 eV for metal hydroxide (M-OH) bonds [41] Figure 4.2 (d). The above XPS analysis further confirms that the formed compound is a bimetallic cobalt tungstate nanoparticle.

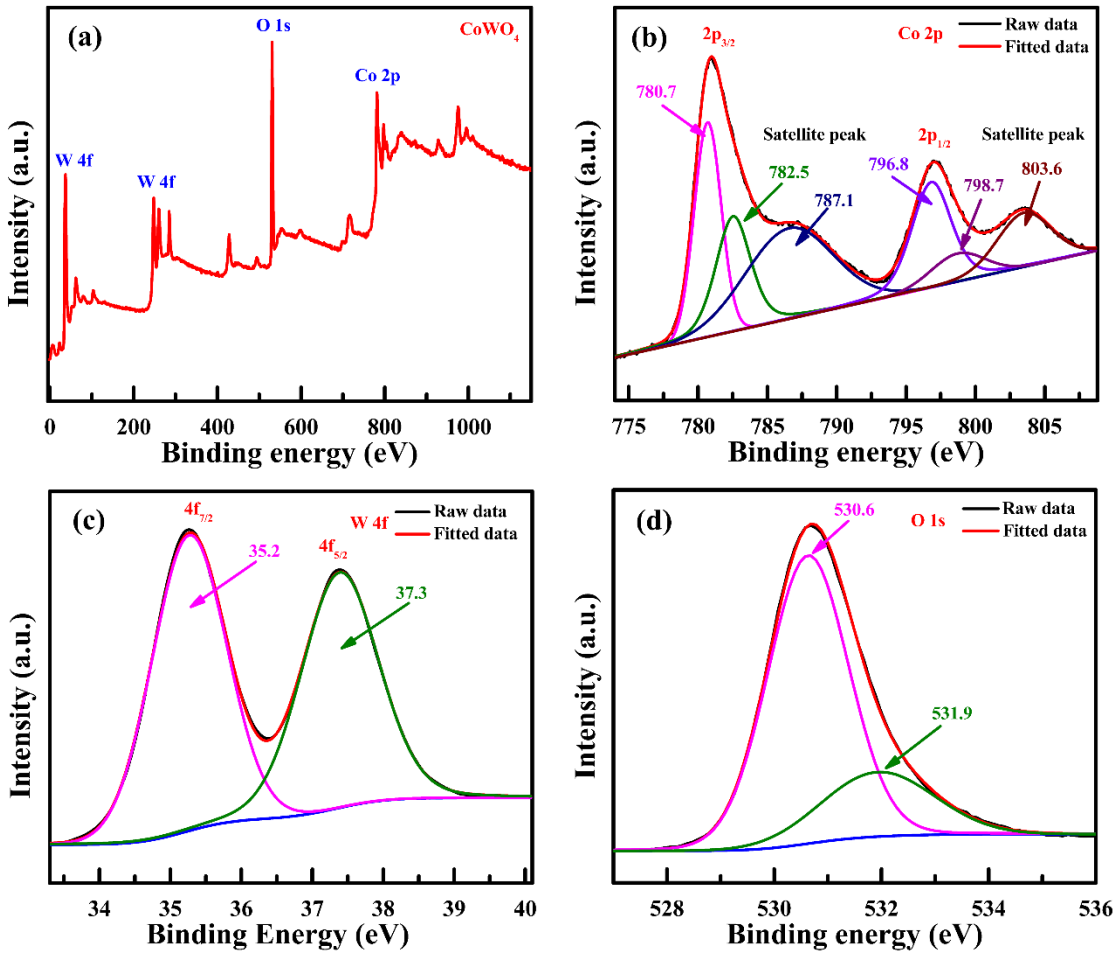

Figure 4.2 XPS survey spectra of $CoWO_4$ nanoparticles (a) and binding energies of Co 2p (b), W 4f (c), and O 1s (d).

The morphology of the synthesized cobalt tungstate nanoparticles was examined by SEM, which is shown in Figure 4.3. In Figure 4.3 (a), the almost sphere-shaped cobalt tungstate nanoparticles in dense amounts and agglomerated nanoparticles can also be seen. The presence of cobalt, tungsten, and oxygen elements and their composition was also

confirmed by EDX analysis. No additional element was found in the EDX spectra, demonstrating the high purity of the synthesized product shown in Figure 4.3 (b).

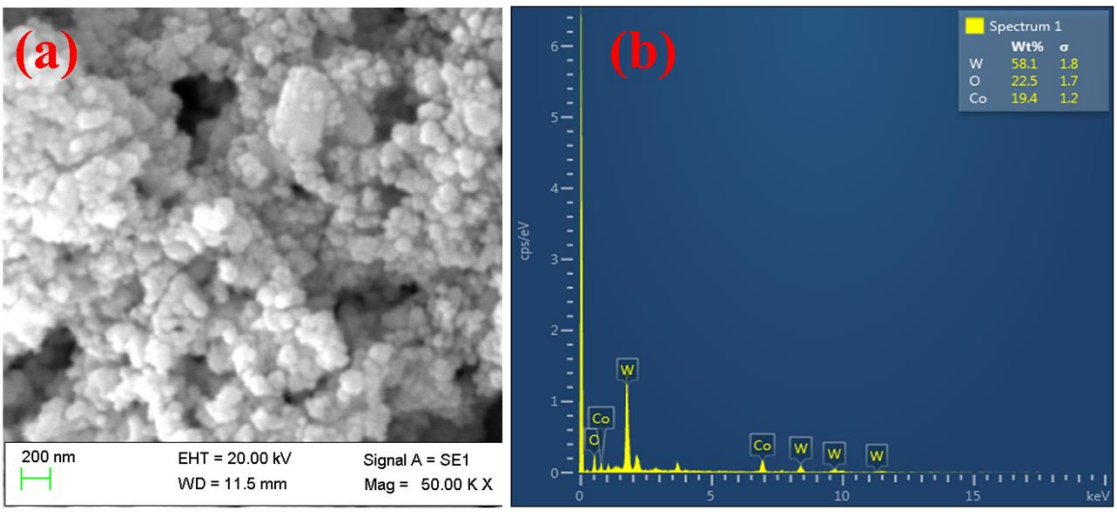

Figure 4.3 (a) SEM image (b) SEM-EDX of $CoWO_4$ nanoparticles.

The inner morphology of the synthesized nanoparticles was further investigated by HR-TEM. Figure 4.4 (a) demonstrates a TEM image of $CoWO_4$ nanoparticles, a sphere-like shape having a diameter of around 30-50 nm. Figure 4.4 (b) shows a clear lattice fringe of the nanoparticles, with an interplanar distance of 0.46 nm and 0.36 nm correlating to the (001) and (011) planes of $CoWO_4$ nanoparticles [42]. In Figure 4.4 (c), the accompanying SAED pattern demonstrates several irregular and continuous intense spots exhibiting the presence of crystalline cobalt tungstate nanoparticles.

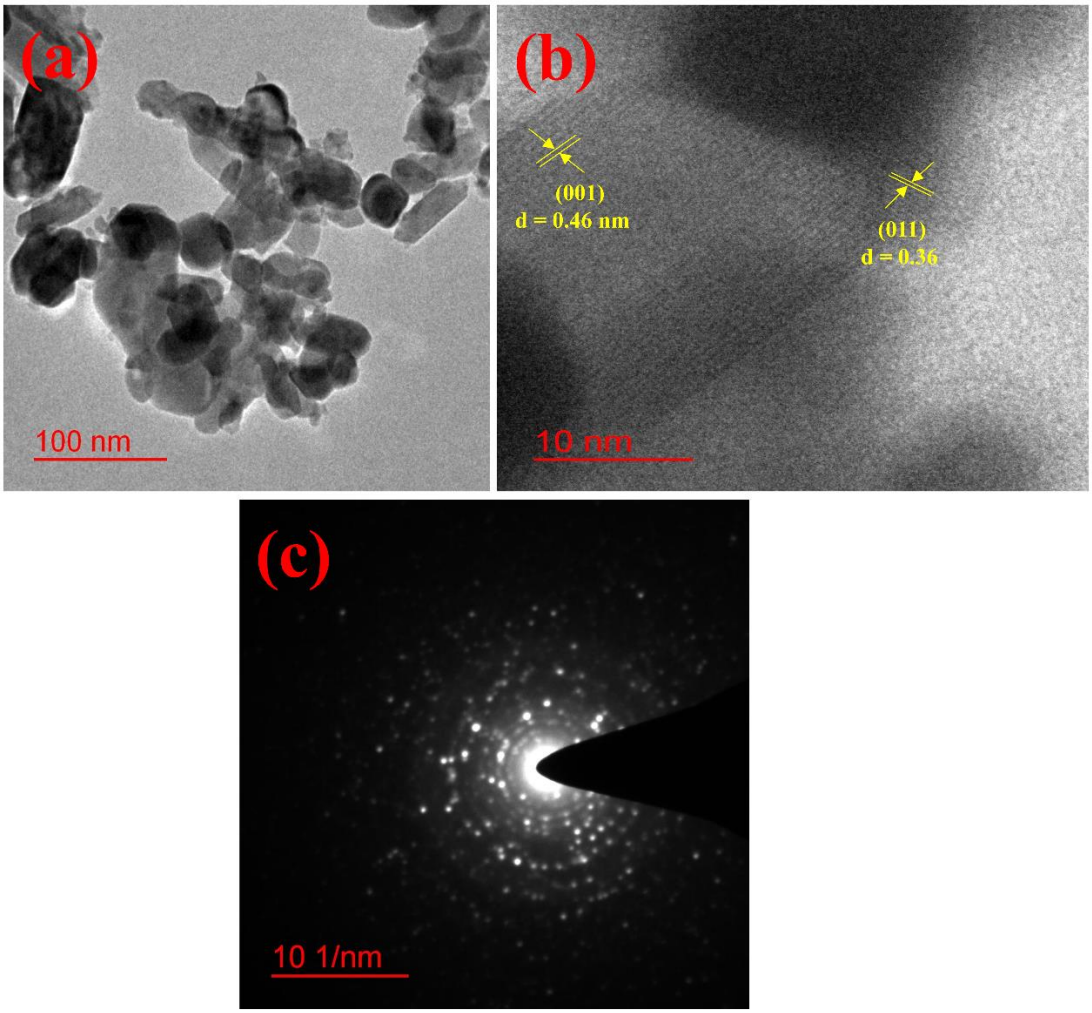

Figure 4.4 (a) TEM image (b) HR-TEM with d-spacing value and (c) SAED pattern of $CoWO_4$ nanoparticles.

4.3.2 Electrochemical oxidation of dopamine at the TCNQ@$CoWO_4$/CPE

The electrochemical behavior of dopamine was studied at TCNQ/CPE and TCNQ@$CoWO_4$/CPE under ideal circumstances. This study was carried out by using the cyclic voltammetry technique in the presence of 100 µM dopamine concentration. Figure 4.5 demonstrates the cyclic voltammetric behavior of bare carbon paste electrode (CPE) (black), TCNQ/CPE (red), and TCNQ@$CoWO_4$ /CPE (blue) in 100 µM dopamine in the presence of 0.1 M phosphate buffer (pH 7.0) at a scan rate of 5 mVs^{-1}. The bare carbon

paste electrode (CPE) did not exhibit any oxidation peak. The TCNQ/CPE and TCNQ@$CoWO_4$/CPE show quasi-reversible redox behavior, and the oxidation peaks were found at 0.29 V and 0.30 V, respectively. The peak-to-peak potential separation value was found to be nearly the same (i.e. 0.25 V) for TCNQ/CPE and TCNQ@$CoWO_4$/CPE, respectively. The oxidation peak current was found to be 9.26 µA for TCNQ/CPE and 19.15 µA for TCNQ@$CoWO_4$/CPE, in which the peak current of TCNQ@$CoWO_4$/CPE is two-fold greater than that of TCNQ/CPE.

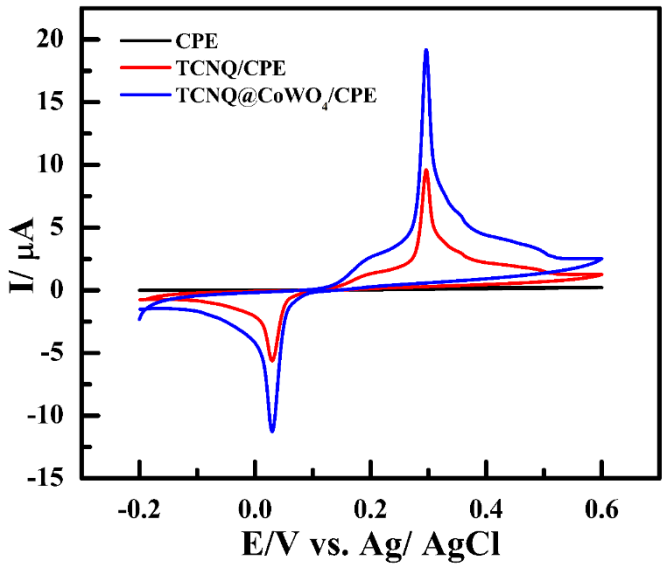

Figure 4.5 Cyclic voltammograms in the presence of 100 µM dopamine in 0.1 M phosphate buffer solution (pH 7.0) at a scan rate of 5 mV/s.

The plausible mechanism of the electrochemical oxidation of dopamine is shown in Figure 4.6.

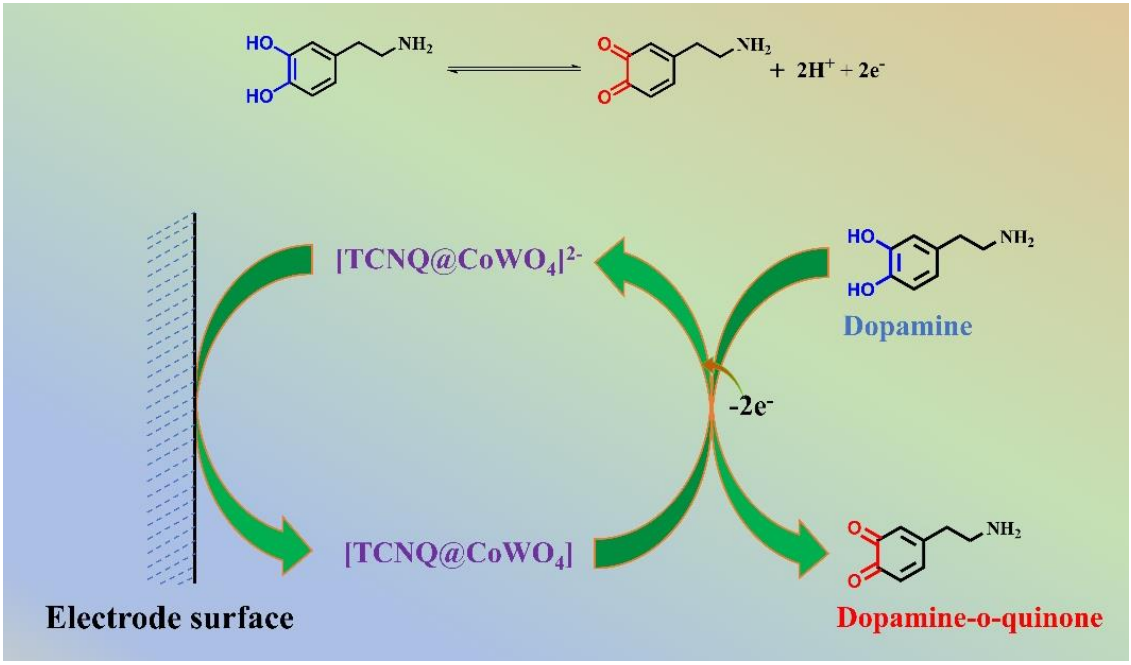

Figure 4.6 Plausible mechanism of electrochemical oxidation of dopamine.

The electrochemical oxidation of dopamine takes place at the electrode surface. During this process, two electrons and two protons are removed, and both electrons are accepted by TCNQ@$CoWO_4$ and converted into $[TCNQ@CoWO_4]^{2-}$. After that, both the electrons are accepted by dopamine-o-quinone and converted into dopamine. This reaction is quasi-reversible in nature, which is confirmed by the cyclic voltammogram, as shown in Figure 4.5.

Figure 4.7 (a) and (b) displays the cyclic voltammetric response of TCNQ/CPE and TCNQ@$CoWO_4$/CPE in 100 µM dopamine-containing 0.1 M phosphate buffer solution at different scan rates from 2 to 250 mVs^{-1}. It is obvious that the anodic (I_{pa}) and the cathodic peak current (I_{pc}) increase when the scan rate increases from 2 to 250 mVs^{-1}. Furthermore, Figure 4.7 (d) demonstrates that the oxidation peak (E_{pa}) and reduction

peak (E_{pc}) potentials exhibit a shift towards higher potential values and lower potential values, respectively, with increasing scan rates. A linear relationship was obtained when we plotted a graph between anodic or cathodic peak current versus the square root of the scan rate was defined as $I_{pa} = 11.34\ \upsilon^{1/2} + 1.779$ ($R^2 = 0.994$) and $I_{pc} = -8.81\ \upsilon^{1/2} + 1.570$ ($R^2 = 0.992$) as shown in Figure 4.7 (d). This linear relationship confirms that the reaction occurring in the presence of dopamine is a diffusion-controlled process.

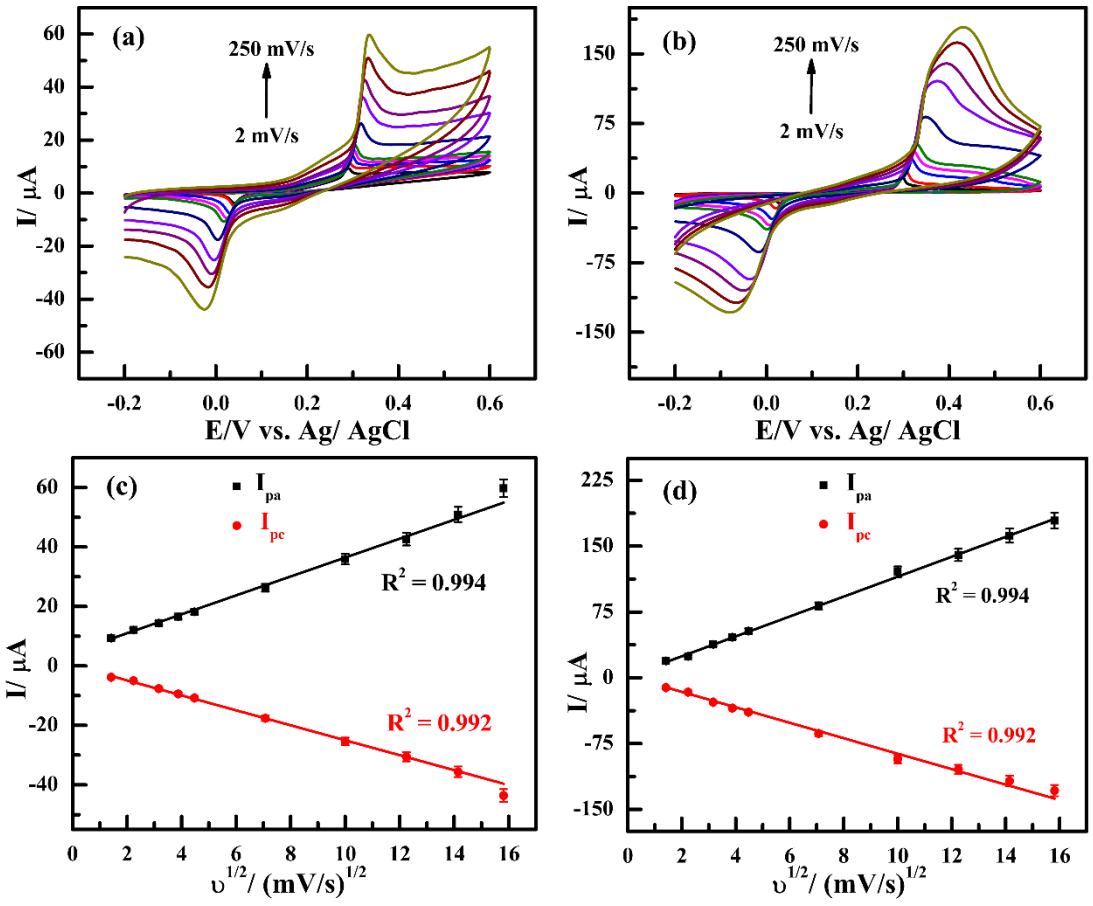

Figure 4.7 Cyclic voltammograms of (a) TCNQ/CPE and (b) TCNQ@$CoWO_4$/CPE at different scan rates 2 to 250 mV/s with 100 µM dopamine. A plot of anodic/cathodic current versus square root of the scan rate for (c) TCNQ/CPE and (d) TCNQ@$CoWO_4$/CPE.

The Randles–Sevcik equation [43-46] was used to calculate the electrochemical active surface area (EASA) of TCNQ/CPE and TCNQ@$CoWO_4$/CPE using equation (4.1)

$$\mathbf{I_p = (2 \cdot 69 * 10^5) n^{3/2} A D^{1/2} \nu^{1/2} C_0} \quad (4.1)$$

Where A is the electrochemically active surface area (cm^2), D is the diffusion coefficient of dopamine (6.0 x 10^{-6} cm^2 s^{-1} at 25 °C), n is the number of electrons involved during the reaction, υ is the scan rate (V/s), I_p is the peak current, and C_0 is the concentration of the electroactive analytes (mol cm^{-3}). Putting these values in equation (4.1), the EASA of TCNQ/CPE and TCNQ@$CoWO_4$/CPE was calculated to be 0.0615 cm^2 and 0.2471 cm^2, respectively. The EASA value demonstrated that TCNQ@$CoWO_4$/CPE has better electrochemical performance than TCNQ /CPE. Therefore, TCNQ@$CoWO_4$/CPE provided an effective platform for the electrochemical oxidation of dopamine. The study revealed the superior capability of TCNQ@$CoWO_4$/CPE based electrode in electron transfer than TCNQ/CPE, validating better conductivity of TCNQ@$CoWO_4$/CPE for dopamine sensing.

4.3.3 Differential pulse voltammetry (DPV) analysis

The differential pulse voltammetry technique was used to analyze dopamine sensing. The dopamine sensing was performed using 0.1 M PBS (pH 7.0), using a potential range between -0.2 V to 0.6 V. Figure 4.8 (a) and (b) exhibit the DPV graphs for dopamine oxidation at various concentrations, ranging from 0 µM to 120 µM for TCNQ/CPE and TCNQ@$CoWO_4$/CPE, respectively. The peak potential for dopamine oxidation was found at around 0.268 V for TCNQ/CPE and 0.274 V for TCNQ@$CoWO_4$/CPE. The magnitude of the peak current increases with increasing the concentration of dopamine.

Figure 4.8 (c) and (d) shows the calibration curve of current versus dopamine concentration for TCNQ/CPE and TCNQ@$CoWO_4$/CPE, respectively. A linear relation was obtained, which further confirms that the reaction in the presence of dopamine is a diffusion-controlled process.

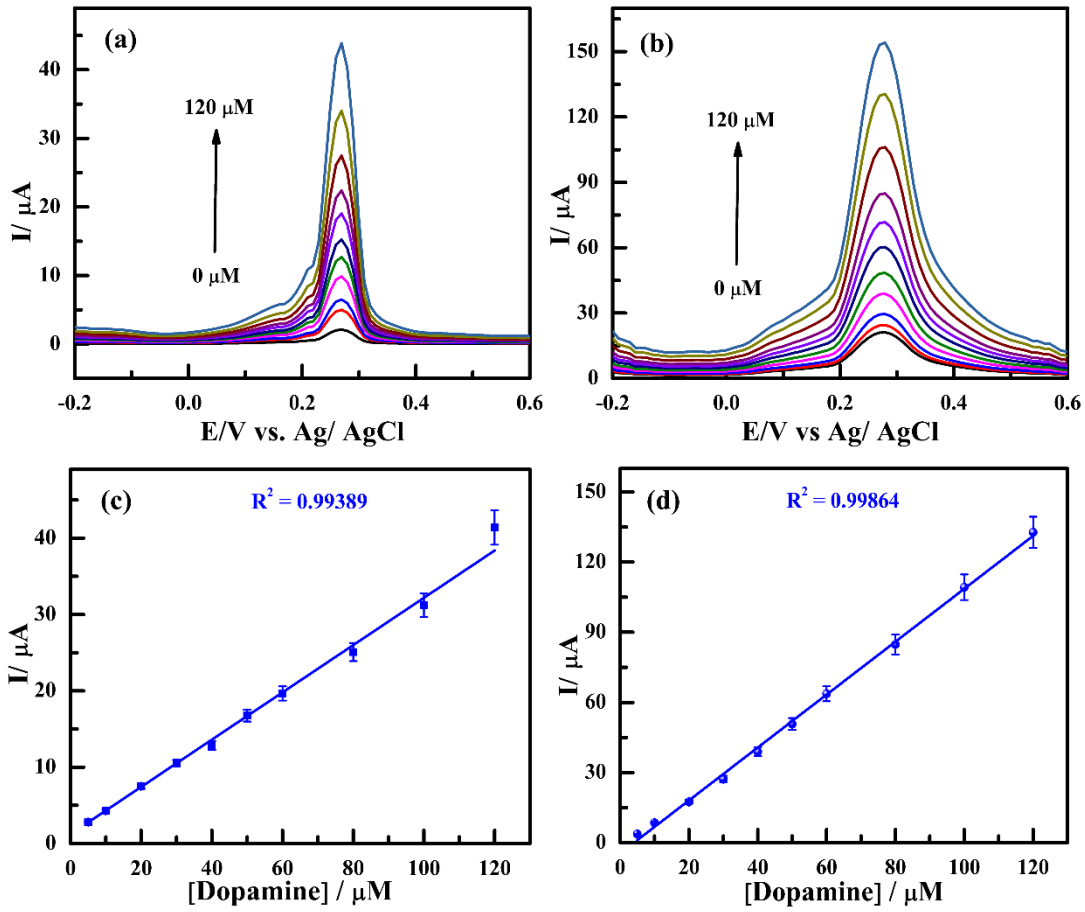

Figure 4.8 DPV curves of (a) TCNQ/CPE and (b) TCNQ@$CoWO_4$/CPE at different concentrations 0 to 120 μM. Calibration curves of current versus concentration of dopamine for (c) TCNQ/CPE and (d) TCNQ@$CoWO_4$/CPE.

4.3.4 Electrochemical impedance spectroscopy (EIS) analysis

The interface characteristics of the modified carbon paste electrodes were further evaluated using electrochemical impedance spectroscopy (EIS) in the presence of 100

µM dopamine. The EIS data was fitted on R(CR)W circuit by using ZSimpWin software. In electrochemical impedance spectroscopy, at higher frequencies, the semicircle part corresponds to the electron transfer process or charge transfer resistance (R_{ct}). While at a lower frequency linear part corresponds to the diffusion control process or mass transfer process. As shown in Figure 4.9, the R_{ct} value is 1950 Ω cm^2 for TCNQ/CPE. When we use TCNQ@$CoWO_4$/CPE, the R_{ct} value is 950 Ω cm^2, decreased compared to the TCNQ/CPE, which confirms that the transfer of electrons is increased at the electrode surface of TCNQ@$CoWO_4$/CPE. This increased electron transfer at the electrode surface is due to the synergistic interaction between $CoWO_4$ and TCNQ.

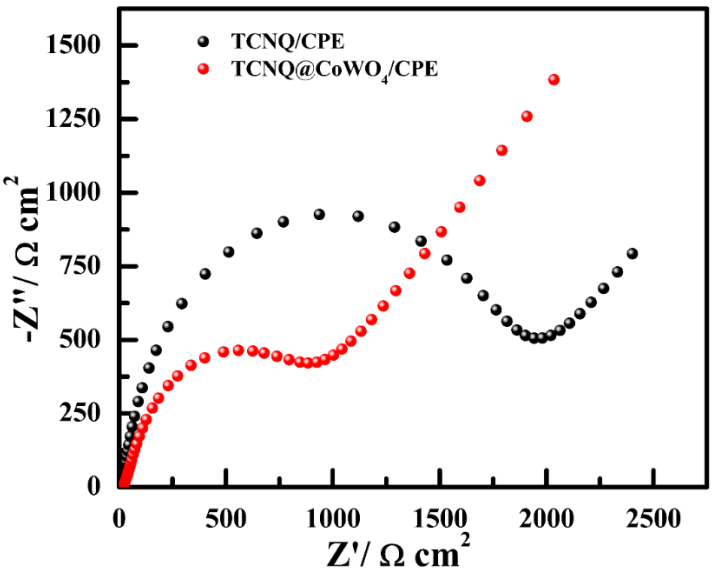

Figure 4.9 Nyquist plots in 0.1 M phosphate buffer solution (pH 7.0) in the presence of 100 µM dopamine at a frequency range between 1 Hz to 1000 kHz.

4.3.5 Amperometric analysis

The amperometric analysis of dopamine was further carried out using 0.1 M phosphate buffer solution (pH 7.0) at an applied potential of 0.29 V vs. Ag/AgCl. Figure 4.10 (a)

and (b) illustrates the current versus time (i-t) response at TCNQ/CPE and TCNQ@$CoWO_4$/CPE by incremental addition of dopamine at varying concentrations ranging from 2 µM to 80 µM. A gradual increase in the oxidation current was observed. At the same time, the sensor achieved 96 to 99% steady-state current in less than 3 seconds, demonstrating a quick amperometric response to dopamine. Based on the findings shown in Figure 4.10 (a) and (b), it can be seen that the current response of the TCNQ/CPE and TCNQ@$CoWO_4$/CPE displayed a direct linear relationship with the concentration of dopamine displayed in Figure 4.10 (c) and (d), respectively. This relationship can be mathematically described by the equation I = 0.18285 * C + 1.34587, with a correlation coefficient of 0.999, where I represents the current in microampere (µA), and C denotes the concentration of dopamine in micromolar (µM). The limit of detection was calculated to be 19.71 µM for TCNQ/CPE and 4.55 µM for TCNQ@$CoWO_4$/CPE at the signal-to-noise ratio three by using the equation (4.2) [47].

$$\mathbf{LOD = 3 * SD/m} \tag{4.2}$$

Where SD is the standard deviation in intercept and m is the slope of the calibration curve. The sensitivity was to be 0.0680 µA/µM and 0.2028 µA/µM for TCNQ/CPE and TCNQ@$CoWO_4$/CPE, respectively. In addition, Table 4.2 provides a summary of a comparison between the detecting performance of this sensor with many other electrochemical dopamine sensors. It is evident from Table 4.2 that the TCNQ@$CoWO_4$ modified carbon paste electrode is able to provide high sensitivity a lower detection limit and a broad linear range so it is superior to the previously reported dopamine sensor.

These characteristics are related to the synergistic effects of TCNQ and $CoWO_4$, which provide enhanced electrocatalytic activity and efficient electron transfer.

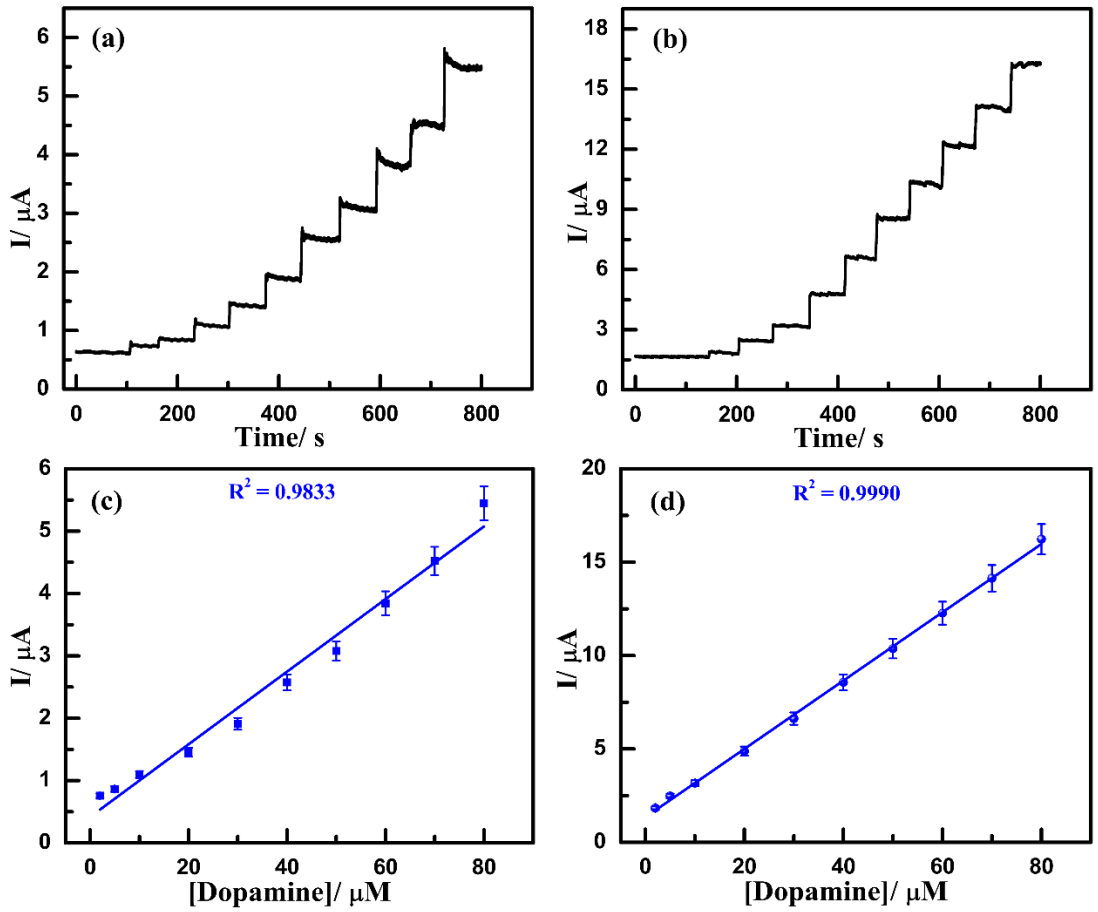

Figure 4.10 Amperometric analyses of (a) TCNQ/CPE and (b) TCNQ@$CoWO_4$/CPE at different concentrations 2 to 80 μM. Calibration curves of current versus concentration of dopamine for (c) TCNQ/CPE and (d) TCNQ@$CoWO_4$/CPE.

Table 4.2 Comparison of sensitivity and detection limit of designed TCNQ@$CoWO_4$/CPE with previously reported electrode value for dopamine detection.

Working electrode	**Linear range (μM)**	**Sensitivity (μA mM^{-1})**	**Detection limit (μM)**	**References**
TCNQ@$CoWO_4$/CPE	2-80	0.202	4.55	This work
TCNQ/CPE	2-80	0.0680	19.71	This work
Ni-Co/GCE	10-500	-	8.20	[48]
Cylindrical AuNEs	1-100	-	5.83	[49]
PrGO/PB/GCE	40-2330	-	26.20	[50]
Nanostructured Gold	10-100	0.139	9.20	[51]
MB/RGO/GCE	15-268	-	5.90	[52]
LDH/CILE	10-1100	-	5.00	[53]
PoPD/E-RGO/GCE	10-400	-	7.50	[54]
AgNPs/rGO	10-800	0.390	5.40	[55]
CDQs/CuO	10-180	-	25.40	[56]
PANI-NF/Pt	62.5-603	-	33.30	[57]
Nano-Au/SAMs gold electrode	200-1200	-	90.00	[58]
Cu nanoplate/GCE	200-2210	-	62.40	[59]
GCE/OLC-CNF	3-11	0.156	1.38	[60]
GCE/Ag-Pt/pCNFs	10-500	0.158	0.11	[61]
GR/Poly (Eb)/CPE	5-110	-	6.52	[62]
Au/ATP-ABA/GCE	15-130	-	9.20	[63]
h-BCN/carbon cloth	10-300	0.140	5.00	[64]

(PB = Prussian blue, MB = methylene blue, LDH = layered double hydroxide, CIIE = carbon ionic liquid electrode, PoPD = Poly(o-Phenylenediamine, NF = nanofiber, SAMs = self-assembled monolayer, OLC-CNF = onion like carbons-carbon nanofiber, GR/Poly (Eb) = graphene/poly (Evan's blue), h-BCN = hexagonal boron carbon nitride).

4.3.6 Effect of pH on TCNQ@$CoWO_4$/CPE

The pH value of the buffer solution is an essential parameter that influences the electrochemical responses of dopamine. The electrochemical response of dopamine was investigated using the cyclic voltammetry technique in 0.1 M phosphate buffers with varying pH levels (ranging from pH 5.0 to pH 9.0). The research findings demonstrate that a maximum oxidation peak current of dopamine was detected at pH 7.0. Furthermore, it was noted that the peak current reduced when there were alterations in the pH value, as shown in Figure 4.11 (a).

4.3.7 Interference, stability, and reproducibility of TCNQ@$CoWO_4$/CPE

The inspection of developed sensors in the presence of interferent molecules is crucial since selectivity is an essential prerequisite for all sensors. The interference study of the TCNQ@$CoWO_4$/CPE-modified electrode was confirmed using amperometric measurement in the presence of a 25 µM dopamine concentration. The findings demonstrated that the electrode exhibited a notable sensitivity towards dopamine and had the capacity to selectively and accurately detect it when other competing biomolecules, such as glucose, KCl, and uric acid are present as shown in Figure 4.11 (b).

The efficiency, stability, and reproducibility of electrodes are crucial factors in electrochemical sensing. Hence, the analysis of the operational stability of TCNQ@$CoWO_4$/CPE was carried out by storing the fabricated sensor to storage at ambient temperature for durations of 5, 10, and 15 days, followed by its evaluation in the

presence of dopamine. The oxidative peak current observed at a concentration of 100 µM dopamine remains relatively constant, indicating a high level of efficiency and stability of the TCNQ@$CoWO_4$/CPE (Figure 4.11 (c)).

The reproducibility of the modified sensor was also examined by the cyclic voltammetry technique in the presence of 100 µM dopamine using five different TCNQ@$CoWO_4$/CPE of the same composition by the same methods. The result of all five electrodes was nearly the same, and the standard deviation was 0.38 % as in Figure 4.11 (d). The finding results disclose a high level of reproducibility for the dopamine sensor.

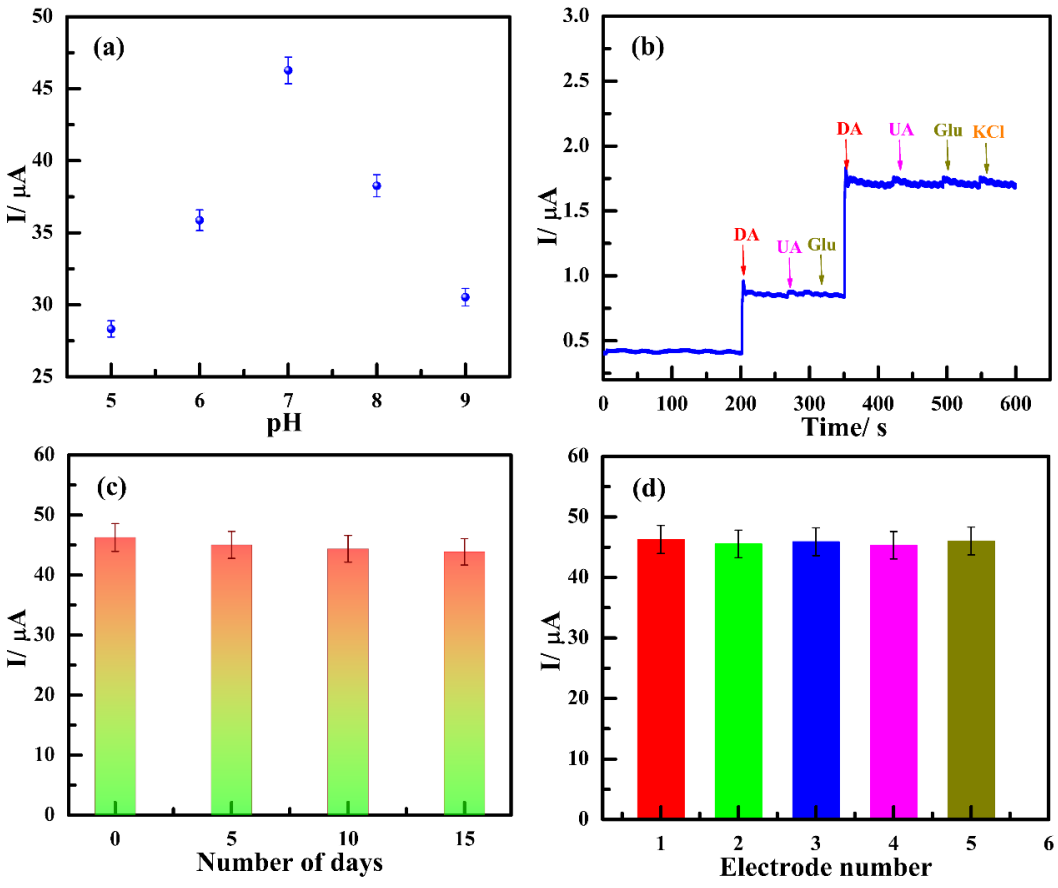

Figure 4.11 (a) Effect of pH on TCNQ@$CoWO_4$/CPE (b) interference (c) stability, and (d) reproducibility of TCNQ@$CoWO_4$/CPE.

4.3.8 Challenges faced during electrochemical sensing of dopamine

Electrochemical sensing of dopamine has some limitations which are discussed below: During electrochemical sensing stability of the electrode is a key issue. The composition of electrode materials such as TCNQ, $CoWO_4$, and binder. The binder plays an important role in the stability of the electrode. If the amount of binder is more then it decreases the current by suppressing the interaction of the analyte to the electrode surface. If the amount of binder is less then fouling of the electrode may take place. To overcome this problem a proper ratio of electrode material and binder should be used. The amount of binder may vary on the electrode material used. The scan rate also affects the stability of the electrode. At a higher scan rate, the delamination of electrodes takes place which decreases the electron transfer and low limit of detection. To overcome this problem, use a lower scan rate. pH of buffer solution also plays an important role in the stability of the electrode. At higher (above 9.0 pH) and lower pH (below 5.0 pH), the electrode starts to delaminate. The use of 0.1 M phosphate buffer solution of pH (7.0) successfully resolves this problem.

However, during electrochemical sensing of dopamine, we have used commercially available dopamine hydrochloride injection in which interfering biomolecules were not present.

Dopamine aqueous solution faces some challenges. The freshly prepared aqueous solution of dopamine after some time gets oxidized at neutral pH. It is stable in the pH range between (pH 3-6). So, the storage of the sample solution for long-term usability is a challenging task. To overcome these problems, we can maintain the pH of the solution between (pH 3-6) which minimizes the oxidation of dopamine. Purging the inert gases

into the sample solution to reduce the oxidation of dopamine in the presence of air. We can store dopamine solutions at low temperatures (4 °C or below) to slow down oxidative and enzymatic processes.

4.3.9 Real sample analysis

The practical application of the TCNQ@$CoWO_4$/CPE sensor was determined by performing real sample analysis on dopamine hydrochloride injection using the standard addition method. The dopamine hydrochloride injection was diluted in 0.1 M phosphate buffer. Dopamine hydrochloride injection samples were spiked with 10, 20, and 50 µM dopamine in 0.1 M phosphate buffer using an amperometric technique at a potential of 0.29 V. The findings of the recovery analysis are shown in Table 4.3, indicating that the average recovery rate for dopamine in dopamine hydrochloride injection was determined to be 95.6 % to 99.36 %. The result indicated that the fabricated sensor has good capability and reliability to recognize real sample analysis with high precision.

Table 4.3 Real sample analysis of dopamine in dopamine hydrochloride injection.

Sample No	**Amount Used (µM)**	**Amount *Found (µM)**	**Recovery (%)**
1	10	9.67 ± 0.14	96.20
2	20	19.49 ± 0.75	95.60
3	50	50.12 ± 0.62	99.36

*Repeated 3 times (n=3)

4.4 Conclusions

This study presents the successful fabrication of a sensitive and selective electrochemical sensor for the detection of dopamine by utilizing TCNQ and $CoWO_4$ nanoparticles. Compared with previously modified electrodes, the TCNQ@$CoWO_4$/CPE exhibited a reduced oxidation potential and greater sensitivity toward dopamine. The constructed dopamine sensor also demonstrated excellent selectivity in the appearance of uric acid, glucose, and potassium chloride. In addition, the real sample analysis was performed by using dopamine hydrochloride injection, and a good recovery result was obtained. Therefore, TCNQ@$CoWO_4$/CPE can be used for precise and selective analysis of dopamine in pharmaceutical samples as a future prospective.

4.5 References

[1] S. Rostami, A. Mehdinia, A. Jabbari, E. Kowsari, R. Niroumand, T.J. Booth, Colorimetric sensing of dopamine using hexagonal silver nanoparticles decorated by task-specific pyridinum based ionic liquid, Sens Actuators B Chem 271 (2018) 64–72. https://doi.org/10.1016/j.snb.2018.05.116.

[2] J. Zhao, W. Zhang, P. Sherrell, J.M. Razal, X.F. Huang, A.I. Minett, J. Chen, Carbon nanotube nanoweb-bioelectrode for highly selective dopamine sensing, ACS Appl Mater Interfaces 4 (2012) 44–48. https://doi.org/10.1021/am201508d.

[3] A. Manbohi, S.H. Ahmadi, Sensitive and selective detection of dopamine using electrochemical microfluidic paper-based analytical nanosensor, Sens Biosensing Res 23 (2019) 100270. https://doi.org/10.1016/j.sbsr.2019.

[4] D. Butler, D. Moore, N.R. Glavin, J.A. Robinson, A. Ebrahimi, Facile Post-deposition Annealing of Graphene Ink Enables Ultrasensitive Electrochemical Detection of Dopamine, ACS Appl Mater Interfaces 13 (2021) 11185–11194. https://doi.org/10.1021/acsami.0c21302.

[5] C. Zhang, X. You, Y. Li, Y. Zuo, W. Wang, D.D. Li, S.W. Huang, H. Hu, F. Yuan, F. Shao, M. Yin, A novel electrochemical aptasensor for serum dopamine detection based on methylene blue-integrated m-PdNFs signal material, Sens Actuators B Chem 354 (2022) 131233. https://doi.org/10.1016/j.snb.2021.

[6] R. Zhao, D. Li, N. Yin, Z. Guo, D. Wang, X. Yao, The high sensitive and selective detection of dopamine based on its electropolymerization by electrochemical surface plasmon resonance, Sens Actuators B Chem 370 (2022) 132401. https://doi.org/10.1016/j.snb.2022..

[7] Y. Zhou, H. Yan, Q. Xie, S. Huang, J. Liu, Z. Li, M. Ma, S. Yao, Simultaneous analysis of dopamine and homovanillic acid by high-performance liquid chromatography with wall-jet/thin-layer electrochemical detection, Analyst 138 (2013) 7246–7253. https://doi.org/10.1039/c3an01437a.

[8] B. Aswathy, G. Sony, Cu2+ modulated BSA-Au nanoclusters: A versatile fluorescence turn-on sensor for dopamine, Microchemical Journal 116 (2014) 151–156. https://doi.org/10.1016/j.microc.2014.04.016.

[9] T. Goswami, A. Bheemaraju, A. Kataria, A. Nag, K. Sravani, S. Mishra, A.K. Mishra, Highly fluorescent water-soluble PTCA incorporated silver nano-cluster for sensing of dopamine, Mater Chem Phys 259 (2021) 124086. https://doi.org/10.1016/j.matchemphys.2020.

[10] Q. Fu, C. Wang, J. Chen, Y. Wang, C. Li, Y. Xie, P. Zhao, J. Fei, BiPO4/BiOCl/g-C3N4 heterojunction based photoelectrochemical sensing of dopamine in serum samples, Colloids Surf A Physicochem Eng Asp 656 (2023) 130456. https://doi.org/10.1016/j.colsurfa.2022.

[11] K. Dashtian, S. Hajati, M. Ghaedi, Ti-Based Solid-State Imprinted-Cu2O/CuInSe2 Heterojunction Photoelectrochemical platform for Highly Selective Dopamine Monitoring, Sens Actuators B Chem 326 (2021) 128824. https://doi.org/10.1016/j.snb.2020.

[12] U. Nishan, R. Gul, N. Muhammad, M. Asad, A. Rahim, M. Shah, J. Iqbal, J. Uddin, A. ul H. Ali Shah, S. Shujah, Colorimetric based sensing of dopamine using ionic liquid functionalized drug mediated silver nanostructures, Microchemical Journal 159 (2020) 105382. https://doi.org/10.1016/j.microc.2020.

[13] X. Zhao, S. Zhao, S. Li, X. Yao, X. Zhu, W. Chen, G. Fan, Z. Liu, Q. Liu, K. Yue, CoO Nanotubes Loaded on Graphene and Modified with Porphyrin Moieties for Colorimetric Sensing of Dopamine, ACS Appl Nano Mater 4 (2021) 8706–8715. https://doi.org/10.1021/acsanm.1c01205.

[14] Y. Sun, Y. Lin, C. Ding, W. Sun, Y. Dai, X. Zhu, H. Liu, C. Luo, An ultrasensitive and ultraselective chemiluminescence aptasensor for dopamine detection based on aptamers modified magnetic mesoporous silica @ graphite oxide polymers, Sens Actuators B Chem 257 (2018) 312–323. https://doi.org/10.1016/j.snb.2017.10.171.

[15] M. Kolahdouz, B. Xu, A.F. Nasiri, M. Fathollahzadeh, M. Manian, H. Aghababa, Y. Wu, H.H. Radamson, Carbon-Related Materials: Graphene and Carbon Nanotubes in Semiconductor Applications and Design, Micromachines (Basel) 13 (2022) 1257. https://doi.org/10.3390/mi13081257.

[16] G. Feng, Y. Yang, J. Zeng, J. Zhu, J. Liu, L. Wu, Z. Yang, G. Yang, Q. Mei, Q. Chen, F. Ran, Highly sensitive electrochemical determination of rutin based on the synergistic effect of 3D porous carbon and cobalt tungstate nanosheets, J Pharm Anal 12 (2022) 453–459. https://doi.org/10.1016/j.jpha.2021.09.007.

[17] S. Rajagopal, D. Nataraj, O.Y. Khyzhun, Y. Djaoued, J. Robichaud, D. Mangalaraj, Hydrothermal synthesis and electronic properties of FeWO4 and CoWO4 nanostructures, J Alloys Compd 493 (2010) 340–345. https://doi.org/10.1016/j.jallcom.2009.12.099.

[18] V. Vinothkumar, R. Sakthivel, S.M. Chen, T.H. Kim, Facile design of wolframite type CoWO4 nanoparticles: A selective and simultaneous electrochemical detection of quercetin and rutin, Journal of Electroanalytical Chemistry 922 (2022) 116774. https://doi.org/10.1016/j.jelechem.2022.116774.

[19] S.S. Patil, U.M. Chougale, R.K. Kambale, V.J. Fulari, Hydrothermal synthesis of CoWO4 nanoparticles and evaluation of their supercapacitive performance, J Energy Storage 67 (2023) 107517. https://doi.org/10.1016/j.est.2023.

[20] P. Taneja, S. Sharma, A. Umar, S.K. Mehta, A.O. Ibhadon, S.K. Kansal, Visible-light driven photocatalytic degradation of brilliant green dye based on cobalt tungstate (CoWO4) nanoparticles, Mater Chem Phys 211 (2018) 335–342. https://doi.org/10.1016/j.matchemphys.2018.02.041.

[21] H.V.S.B. Azevêdo, R.A. Raimundo, L.S. Ferreira, M.M.S. Silva, M.A. Morales, D.A. Macedo, U.U. Gomes, D.G.L. Cavalcante, Green synthesis of CoWO4 powders using agar-agar from red seaweed (Rhodophyta): Structure, magnetic properties and battery-like behavior, Mater Chem Phys 242 (2020) 122544. https://doi.org/10.1016/j.matchemphys.2019.

[22] P.P. Bagwade, D.B. Malavekar, S.B. Ubale, R.N. Bulakhe, I. In, U.M. Patil, C.D. Lokhande, Synthesis, characterization and supercapacitive application of nanocauliflower-like cobalt tungstate thin films by successive ionic layer adsorption and reaction (SILAR) method, Electrochim Acta 408 (2022) 139933. https://doi.org/10.1016/j.electacta.2022.

[23] V. Vinothkumar, R. Sakthivel, S.M. Chen, T.H. Kim, Facile design of wolframite type CoWO4 nanoparticles: A selective and simultaneous electrochemical detection of quercetin and rutin, Journal of Electroanalytical Chemistry 922 (2022) 116774. https://doi.org/10.1016/j.jelechem.2022.

[24] S.M. Alshehri, J. Ahmed, T. Ahamad, P. Arunachalam, T. Ahmad, A. Khan, Bifunctional electro-catalytic performances of CoWO4 nanocubes for water redox reactions (OER/ORR), RSC Adv 7 (2017) 45615–45623. https://doi.org/10.1039/c7ra07256b.

[25] Y.L. Oliveira, A.F. Gouveia, M.J.S. Costa, F.H.P. Lopes, J.C. Sczancoski, E. Longo, G.E. Luz, R.S. Santos, L.S. Cavalcante, Investigation of electronic structure, morphological features, optical, colorimetric, and supercapacitor electrode properties of CoWO4 crystals, Mater Sci Energy Technol 5 (2022) 125–144. https://doi.org/10.1016/j.mset.2021.12.006.

[26] Z. Song, J. Ma, H. Sun, Y. Sun, J. Fang, Z. Liu, C. Gao, Y. Liu, J. Zhao, Low-temperature molten salt synthesis and characterization of CoWO4 nano-particles, Mater Sci Eng B Solid State Mater Adv Technol 163 (2009) 62–65. https://doi.org/10.1016/j.mseb.2009.05.002.

[27] S. Shanmugapriya, S. Surendran, V.D. Nithya, P. Saravanan, R. Kalai Selvan, Temperature dependent electrical and magnetic properties of CoWO4 nanoparticles synthesized by sonochemical method, Mater Sci Eng B Solid State Mater Adv Technol 214 (2016) 57–67. https://doi.org/10.1016/j.mseb.2016.09.002.

[28] R. Dhilip Kumar, S. Karuppuchamy, Microwave mediated synthesis of nanostructured Co -WO3 and CoWO4 for supercapacitor applications, J Alloys Compd 674 (2016) 384–391. https://doi.org/10.1016/j.jallcom.2016.03.074.

[29] A. Li, Y. Tu, Y. Zhu, D. Li, W. Zhou, X. Zhu, L. Feng, CoWO4 nanoparticles prepared in different solvents and their pseudocapacitant performances, Int J Electrochem Sci 12 (2017) 5646–5656. https://doi.org/10.20964/2017.06.60.

[30] S. Thongtem, S. Wannapop, T. Thongtem, Characterization of CoWO4 nano-particles produced using the spray pyrolysis, Ceram Int 35 (2009) 2087–2091. https://doi.org/10.1016/j.ceramint.2008.11.014.

[31] S. Sagadevan, J. Podder, I. Das, Synthesis and characterization of CoWO4 nanoparticles via chemical precipitation technique, Journal of Materials Science: Materials in Electronics 27 (2016) 9885–9890. https://doi.org/10.1007/s10854-016-5057-5.

[32] S. Rajagopal, D. Nataraj, O.Y. Khyzhun, Y. Djaoued, J. Robichaud, D. Mangalaraj, Hydrothermal synthesis and electronic properties of FeWO4 and CoWO4 nanostructures, J Alloys Compd 493 (2010) 340–345. https://doi.org/10.1016/j.jallcom.2009.12.099.

[33] S. Pourmasoud, M. Eghbali-Arani, V. Ameri, M. Rahimi-Nasrabadi, F. Ahmadi, A. Sobhani-Nasab, Synthesis of some transition MWO 4 (M: Mn, Fe, Co, Ni, Cu, Zn, Cd) nanostructures by hydrothermal method, Journal of Materials Science: Materials in Electronics 30 (2019) 8105–8144. https://doi.org/10.1007/s10854-019-01179-2.

[34] L. Ma, P. Hu, C. Kloc, H. Sun, M.E. Michel-Beyerle, G.G. Gurzadyan, Ultrafast spectroscopic characterization of 7,7,8,8- tetracyanoquinodimethane (TCNQ) and

its radical anion (TCNQ-), Chem Phys Lett 609 (2014) 11–14. https://doi.org/10.1016/j.cplett.2014.06.029.

[35] H. Tamaya, H. Nakano, T. Iimori, 7,7,8,8-Tetracyanoquinodimethane (TCNQ) emits visible photoluminescence in solution, J Lumin 192 (2017) 203–207. https://doi.org/10.1016/j.jlumin.2017.06.051.

[36] T. Iimori (飯森俊文), T. Ishikawa (石川拓), Y. Torii (鳥井悠人), H. Tamaya (玉谷穂菜美), H. Nakano (中野英之), M. Kanno (菅野眞生), Effect of rigidity of microenvironment on fluorescence of 7,7,8,8-tetracyanoquinodimethane (TCNQ), Chem Phys Lett 738 (2020) 136912. https://doi.org/10.1016/j.cplett.2019.

[37] B. Han, R. Ma, H. Wang, M. Zhou, High pressure investigations on TTF-TCNQ charge-transfer complexes, Spectrochim Acta A Mol Biomol Spectrosc 267 (2022) 120541. https://doi.org/10.1016/j.saa.2021.

[38] P. Taneja, S. Sharma, A. Umar, S.K. Mehta, A.O. Ibhadon, S.K. Kansal, Visible-light driven photocatalytic degradation of brilliant green dye based on cobalt tungstate (CoWO4) nanoparticles, Mater Chem Phys 211 (2018) 335–342. https://doi.org/10.1016/j.matchemphys.2018.02.041.

[39] V. Vinothkumar, R. Sakthivel, S.M. Chen, T.H. Kim, Facile design of wolframite type CoWO4 nanoparticles: A selective and simultaneous electrochemical detection of quercetin and rutin, Journal of Electroanalytical Chemistry 922 (2022) 116774. https://doi.org/10.1016/j.jelechem.2022.

[40] B. Li, F. Wei, B. Su, Z. Guo, Z. Ding, M.Q. Yang, S. Wang, Mesoporous cobalt tungstate nanoparticles for efficient and stable visible-light-driven photocatalytic CO2 reduction, Mater Today Energy 24 (2022) 100943. https://doi.org/10.1016/j.mtener.2022.

[41] S.M. Alshehri, J. Ahmed, T. Ahamad, P. Arunachalam, T. Ahmad, A. Khan, Bifunctional electro-catalytic performances of CoWO4 nanocubes for water redox reactions (OER/ORR), RSC Adv 7 (2017) 45615–45623. https://doi.org/10.1039/c7ra07256b.

[42] X. Xu, J. Shen, N. Li, M. Ye, Facile synthesis of reduced graphene oxide/CoWO4 nanocomposites with enhanced electrochemical performances for supercapacitors, Electrochim Acta 150 (2014) 23–34. https://doi.org/10.1016/j.electacta.2014.10.139.

[43] X. Sun, Y. Yan, Y. Wang, Y. Zhao, X. Dou, D. Zhang, L. Lu, G. Guo, X. Wang, Sensitive electrochemical measurement of nitric oxide released from living cells based on dealloyed PtBi alloy nanoparticles, Microchimica Acta 190 (2023) 277. https://doi.org/10.1007/s00604-023-05837-5.

[44] J.N. Baby, B. Sriram, Y.F. Hsu, S.F. Wang, R. Bartholomew, M. George, Rational incorporation of strontium pyrophosphate/hexagonal boron nitride composite for trace level electrochemical sensing of dopamine, Microchemical Journal 183 (2022) 108067. https://doi.org/10.1016/j.microc.2022.

[45] K.K. Maurya, K. Singh, M. Malviya, Effect of palladium and its nanogeometry on the redox electrochemistry of tetracyanoquinodimethane modified electrode; application in electrochemical sensing of ascorbic acid, J Appl Electrochem 53 (2023) 1831–1842. https://doi.org/10.1007/s10800-023-01878-z.

[46] K. Singh, C. Singh, K.K. Maurya, M. Malviya, Redox electrochemistry of electrodes tuned with dimethyl ferrocene based on Co–NC–Pd nanogeometry: an impedimetric sensor for NADH sensing, Journal of Materials Science: Materials in Electronics 34 (2023) 1898. https://doi.org/10.1007/s10854-023-11257-1.

[47] C. Direksilp, J.M. Scheiger, N. Ariyasajjamongkol, A. Sirivat, A highly selective and sensitive electrochemical sensor for dopamine based on a functionalized multi-walled carbon nanotube and poly(: N -methylaniline) composite, Analytical Methods 14 (2022) 469–479. https://doi.org/10.1039/d1ay01943k.

[48] C. Yang, X. Sun, C. Zhang, M. Liu, Green synthesis of Co-Ni hollow spheres for its electrochemical detection of dopamine, Journal of Nanoparticle Research 22 (2020) 55. https://doi.org/10.1007/s11051-020-4775-z.

[49] D.S. Kim, E.S. Kang, S. Baek, S.S. Choo, Y.H. Chung, D. Lee, J. Min, T.H. Kim, Electrochemical detection of dopamine using periodic cylindrical gold nanoelectrode arrays, Sci Rep 8 (2018) 14049. https://doi.org/10.1038/s41598-018-32477-0.

[50] P.L. dos Santos, V. Katic, K.C.F. Toledo, J.A. Bonacin, Photochemical one-pot synthesis of reduced graphene oxide/Prussian blue nanocomposite for simultaneous electrochemical detection of ascorbic acid, dopamine, and uric acid, Sens Actuators B Chem 255 (2018) 2437–2447. https://doi.org/10.1016/j.snb.2017.09.036.

[51] B.J. Plowman, M. Mahajan, A.P. O'Mullane, S.K. Bhargava, Electrochemical detection of dopamine and cytochrome c at a nanostructured gold electrode,

Electrochim Acta 55 (2010) 8953–8959. https://doi.org/10.1016/j.electacta.2010.08.045.

[52] H. Wang, T. Cao, Y. Zhou, L. Liu, X. Zhang, Z. Tong, A facile approach to synthesis methylene blue/reduced graphene oxide nanocomposite and simultaneous determination of dopamine and uric acid, J Appl Electrochem 52 (2022) 1067–1080. https://doi.org/10.1007/s10800-022-01695-w.

[53] Z. Zhu, L. Qu, Y. Guo, Y. Zeng, W. Sun, X. Huang, Electrochemical detection of dopamine on a Ni/Al layered double hydroxide modified carbon ionic liquid electrode, Sens Actuators B Chem 151 (2010) 146–152. https://doi.org/10.1016/j.snb.2010.09.032.

[54] X. Liu, H. Zhu, X. Yang, An electrochemical sensor for dopamine based on poly(o-phenylenediamine) functionalized with electrochemically reduced graphene oxide, RSC Adv 4 (2014) 3706–3712. https://doi.org/10.1039/c3ra45234d.

[55] B. Kaur, T. Pandiyan, B. Satpati, R. Srivastava, Simultaneous and sensitive determination of ascorbic acid, dopamine, uric acid, and tryptophan with silver nanoparticles-decorated reduced graphene oxide modified electrode, Colloids Surf B Biointerfaces 111 (2013) 97–106. https://doi.org/10.1016/j.colsurfb.2013.05.023.

[56] S.E. Elugoke, O.E. Fayemi, A.S. Adekunle, B.B. Mamba, T.T.I. Nkambule, E.E. Ebenso, Electrochemical sensor for the detection of dopamine using carbon quantum dots/copper oxide nanocomposite modified electrode, FlatChem 33 (2022) 100372. https://doi.org/10.1016/j.flatc.2022.

[57] H.N. Yu, Y.C. Pang, J.Y. Tang, Polyaniline Nanofiber Modified Platinum Electrode Used to Determination of Dopamine by Square Wave Voltammetry Technique, 10 (2015) 8353-8360. https://doi.org/10.1016/S1452-3981(23)11101-1.

[58] J.B. Raoof, A. Kiani, R. Ojani, R. Valiollahi, S. Rashid-Nadimi, Simultaneous voltammetric determination of ascorbic acid and dopamine at the surface of electrodes modified with self-assembled gold nanoparticle films, Journal of Solid State Electrochemistry 14 (2010) 1171–1176. https://doi.org/10.1007/s10008-009-0917-z.

[59] L. Xu, S. Tang, L. Zhang, J. Du, J. Xu, N. Li, Z. Tang, Preparation of Copper Nanoplates in Aqueous Phase and Electrochemical Detection of Dopamine, Life 12 (2022) 999. https://doi.org/10.3390/life12070999.

[60] O.C. Ozoemena, L.J. Shai, T. Maphumulo, K.I. Ozoemena, Electrochemical Sensing of Dopamine Using Onion-like Carbons and Their Carbon Nanofiber Composites, Electrocatalysis 10 (2019) 381–391. https://doi.org/10.1007/s12678-019-00520-x.

[61] Y. Huang, Y.E. Miao, S. Ji, W.W. Tjiu, T. Liu, Electrospun carbon nanofibers decorated with Ag-Pt bimetallic nanoparticles for selective detection of dopamine, ACS Appl Mater Interfaces 6 (2014) 12449–12456. https://doi.org/10.1021/am502344p.

[62] G.V. Prasad, T.V. Gopal, G. Venkataprasad, T.M. Reddy, P. Shaikshavali, P. Gopal, Fabrication of a Novel Shaped Graphene/poly (Evan's blue) Composite Chemical Sensor for the Electrocatalytic Boost up of Neurotransmitter (Dopamine): A Voltammetric Investigation, 8 (2019) 1100-1116.

[63] L. Zhang, X. Jiang, Attachment of gold nanoparticles to glassy carbon electrode and its application for the voltammetric resolution of ascorbic acid and dopamine, Journal of Electroanalytical Chemistry 583 (2005) 292–299. https://doi.org/10.1016/j.jelechem.2005.06.014.

[64] Y.S. Bi, B. Liu, X.Y. Liu, Y. Qin, B.X. Zou, A h-BCN for electrochemical sensor of dopamine and uric acid, J Nanomater 2020 (2020) 1-9. https://doi.org/10.1155/2020/4604820.